Arch Appl Mech (2012) 82:1423–1437
DOI 10.1007/s00419-012-0667-8

SPECIAL ISSUE

Basit Khalid · Franz Ziegler

A novel aseismic foundation system for multipurpose asymmetric buildings

Received: 30 July 2011 / Accepted: 5 December 2011 / Published online: 27 June 2012

Abstract The vulnerability of civil engineering structures with fundamental frequency, say roughly above 1 Hz, (or buildings having less than ten stories), when exposed to the strong motion phase of an earthquake is considerably reduced by means of base isolation. The low-pass filter for isolating horizontal vibrations is redesigned where the classical elastomeric bearings are substituted by a number of prestressed helical steel springs with pivoted columns along their vertical axes carrying a fraction of the dead weight and guiding the remaining horizontal motion. The base-isolated building in its fundamental mode is considered to be rigid and low-cost tuned liquid column gas dampers (TLCGDs), in optimal arrangement within the plan of the basement of the building, supply the effective damping of the remaining horizontal vibrations. TLCGD-tuning in a first step is performed by a simple transformation of the well-documented optimal parameters of the tuned mass damper (TMD) followed by fine-tuning in state space. The action of the passive damping device is commonly considered to be sufficient. Since the gas-spring effect somewhat counter acts changes in fluid mass, the absorber can be used as a water reservoir. Compatible sliding elements are innovatively designed to resist the motion of the building relative to the ground for sufficiently small disturbances by static friction, thus complete the isolation system. However, during seismic excitation, the frictional contact is released over much of the time to avoid excessive wear.

Keywords Vibration control · Base isolation · Asymmetric buildings · Tuned liquid column gas dampers · Seismic excitation ·

1 Introduction

It is the horizontal component of the strong motion phase of an earthquake that shakes and possibly endangers regular buildings. To reduce the vulnerability of buildings with fundamental frequency higher than about 1 Hz (or buildings with less than 10 stories), base isolation is the best suited. It decouples the structure from ground motions by means of mechanical low-pass filter. The decoupling is achieved by inserting a layer of low horizontal and high vertical stiffness between the superstructure and its foundation. The isolated building thus has a natural frequency in its base isolation mode below about 0.5 Hz, that is, much lower than the fundamental frequency of the fixed-base structure and certainly lower than the predominant frequencies of the expected ground motion. The most common laminated isolation elements consist of alternating layers of steel and rubber that need additional damping usually provided by lead core, hydraulic or mechanical dampers. This element

B. Khalid
Directorate of Civil Engineering and Design, Islamabad, Pakistan
E-mail: basitdotcom@hotmail.com

F. Ziegler (✉)
Vienna University of Technology, Karlsplatz 13, 1040/E2063 Vienna, Austria
E-mail: franz.ziegler@tuwien.ac.at

has a rather large ratio of the vertical to the horizontal stiffness; the latter in a rough approximation is given in terms of the rubber shear modulus, by $k_{1h} = GA/ns_1$, where A and s_1 are, respectively, the cross-sectional area and the thickness of the n-times repeated rubber sheets, for extensive reviews and a novel application to isolate bridges, see [1–9].

There are lifetime problems encountered, mainly caused by the increase in temperature due to alternating plastic deformations of the lead core during the first occurrence of the earthquake or during the aftershocks. Consequently, the isolation element has been recently separated from the sliding element so that the former would serve the isolation solely whereas the latter provides the "required" static friction and, in motion dissipates energy by dry friction, see Bachmann [7] for such an arrangement of isolation (elastomeric) and sliding bearings. Therefore, a novel base isolation system is proposed in this paper to address such lifetime problems. The innovatively designed isolation element, complemented by a separate sliding element and modally tuned liquid column gas dampers (TLCGDs), all invented and described in detail by Khalid [8], constitute the above said foundation system. The isolation element consists of prestressed helical steel springs with pivoted columns along their vertical axes carrying a fraction of the dead weight of the building and thus acts as low-pass filter and as a durable replacement of classical rubber bearing. The sliding elements are designed to provide the required static friction to resist loads by wind gusts and small seismic disturbances (e.g., of traffic origin), but without continuous energy dissipation. The state-of-the-art low-cost TLCGDs are optimally integrated in the basement of the building to supply the effective damping of the isolation modes. An experimental verification is presented in [9], and the new isolation system is partly described in [10,11], such a base isolation system has hardly any maintenance costs and has a lifetime comparable with that of the building. In the design stage of the TLCGD the readily available modally tuned parameters, frequency and damping of tuned mechanical dampers (TMDs), originally derived by Den Hartog [12], by a simple transformation, [13], renders approximately those of the liquid absorber. Fine-tuning is subsequently performed in state space that not only renders the parameter optimal but allows us to divide the absorbers into sets of smaller units in parallel action. The latter absorb and dissipate energy in a much wider frequency window around the resonance frequency of the base-isolated building. We consider the generalized modal coordinates in state space to make the coupling of the first-order equations rather weak namely to solely result from the action of multiple TLCGDs.

2 Equation of motion of the base-isolated building

Due to the low-pass filter placed below the building within its aseismically designed foundation, the horizontal deformations caused by the horizontal component of an earthquake are concentrated in the isolation units, and the resulting (in general three) low-frequency isolation modes can be considered as rigid body motions of the building. This fact has been convincingly approved: for a simple steel frame with classical base isolation, see Chopra [14], p. 403, with novel application of a TLCGD, see again Khalid [8]. The vertical motion of the building is a combination of the vertical component of the seismic ground displacement (no soil structure interaction is considered) with a guided component from its horizontal motion. Consequently, for setting up the equations of the horizontal isolation motion by means of conservation of momentum and of angular momentum about the vertical axis, we need to know the total mass m_S, the moment of inertia $I_x = m_S r_x^2$ and the location of the center of mass C_M in the plan of the building. Hence, three equations result in matrix form, the mass matrix is diagonal, displacements of the center of mass are denoted v_M, w_M, rotation about vertical x-axis is considered in dimension as of length by $u_T = r_x^\theta$. A single point, horizontal seismic excitation by ground acceleration $a_g(t)$ with angle of incidence αagainst y-axis is understood,

$$\underset{\sim}{M}\ddot{\vec{x}} + \underset{\sim}{K}\vec{x} = -\underset{\sim}{M} a_g \vec{e}_g + \vec{F},\ \vec{x}^T = [v_M \quad w_M \quad u_T],\ \vec{e}_g^T = [\cos\alpha \quad \sin\alpha \quad 0] \tag{1}$$

The generalized control force vector $\vec{F}$ supplies the action of the TLCGDs. Substructure synthesis of Eq. (1) with TMDs of the spring-mass-dashpot type would be "exact"; however, that with equivalent TLCGDs becomes approximate since the (small amount) of dead fluid mass changes slightly the location of the center of mass, the mass matrix and thus the main system considered in Eq. (1). Extremely light structural damping of the low-pass filter [not considered in Eq. (1)] will be added to the modally projected equations. Since we can assume isotropic horizontal stiffness of each of the base isolation elements, k_{1h}, and either some equal spacing along the perimeter of the carrying walls of the building or alternatively, a concentration of such elements below the main carrying columns of a frame structure, the symmetric 3×3 stiffness matrix $\underset{\sim}{K}$ of the base isolation is easily set up, for example, by the direct stiffness matrix method, Clough and Penzien [15].

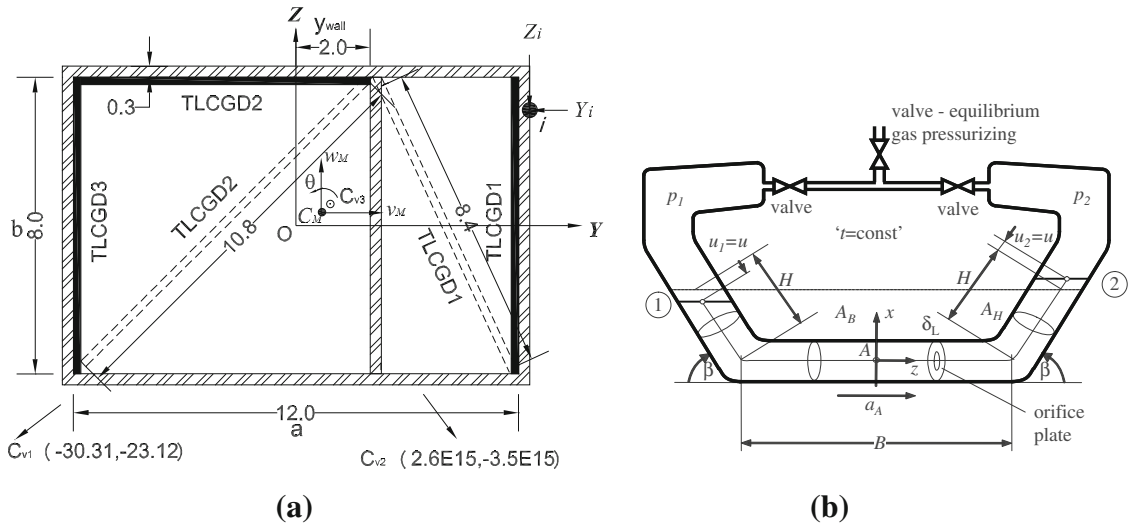

Fig. 1 **a** Plan of an asymmetric building. Restoring spring force of a base isolation element at position i indicated. Suboptimal placements of the three TLCGDs (in two alternatives) relative to the modal centers of velocity C_{vj}, Khalid [8]. **b** New symmetric TLCGD; framed piping system, sealed: each limb has a gas vessel on *top*, kept at equilibrium gas pressure (supplied to both sides through the central valve; side valves are kept closed for sealing in action)

Considering a number N of such base isolation elements, the resulting horizontal stiffness is apparent in the two diagonal stiffness elements of the stiffness matrix, $k_{11} = k_{22} = Nk_{1h}$. Thus, the required isolation period provides a first condition to be met in the design of the base isolation by choosing the resulting stiffness,

$$T = 2\pi\sqrt{m_S/Nk_{1h}} \geq 2\text{s} \tag{2}$$

Considering just for the sake of simplicity of calculations, a simple rectangular plan $a \times b$ of an asymmetric building with an intermediate carrying wall and a symmetric distribution of the isotropic base isolation elements, such that their number is $N = 2N_a + 3N_b$, the third diagonal component and the off-diagonal elements of the stiffness matrix become, Fig. 1a,

$$k_{33} = \frac{Nk_{1h}}{r_x^2}\left[y_M^2 + z_M^2 + \frac{N_b}{2N}\left(a^2 + 2y_{\text{wall}}^2 - 4y_{\text{wall}}y_M\right) + \frac{N_a}{2N}b^2 + \frac{3}{N}\sum_{i=1}^{N_b} z_i^2 + \frac{2}{N}\sum_{i=1}^{N_a} y_i^2\right] \tag{3}$$

$$k_{13} = k_{31} = Nk_{1hz_M}/r_x, k_{32} = k_{23} = Nk_{1h}y_M(N_b y_{\text{wall}}/Ny_M - 1)/r_x$$

Centers of mass and isolation stiffness are distinct points rendering the asymmetry mentioned above.

2.1 Modal analysis of the base-isolated building

Solving the linear eigen-value problem of Eq. (1), for example, by calling the tool *eig* in Matlab [16], renders the set of three orthonormalized modal vectors and the associated natural frequencies, say around 0.5 Hz. The placement of the modally TLCGDs becomes optimal with normal distance to the modal centers of velocity maximum: centers far outside of the building plan indicate dominating translational motion in that mode, whereas dominating modal rotational vibrations render a modal center within the building plan, see [17]. For small displacements, the 3x1 modal displacement vectors $\vec{\phi}_j$, $j = 1, 2$ and 3, determine the three modal centers of velocity C_{vj}, Ziegler [18], p.13, see Fig. 1a,

$$y_{vj} = y_M - r_x\phi_{j2}/\phi_{j3}, z_{vj} = z_M + r_x\phi_{j1}/\phi_{j3}, \phi_{j3} \neq 0 \tag{4}$$

The illustrative base-isolated building, see again Fig. 1a for its plan and dimensions, is a single story "one-family" house. It is selected due to the serious attempts made in "developing countries" in highly seismic risk zones to provide safe (prefabricated) homes of this type; thus, its total mass is $m_S \approx 245,000$ kg and radius of inertia $r_x = 4.65$ m, where $3b/2a = 1$. Adding several stories within those limits given by the

fixed-base fundamental frequency just adds mass but would not influence the qualitative design of the novel base isolation elements. A number $N = 240$ of equidistantly arranged isolation elements as described below suffices, [consequently, $2N_a = 3N_b$ and thus $N_a = 60$, $N_b = 40$ in Eq. (3)], and the natural ortho-normalized isolation modes result

$$\begin{bmatrix} f_1 = 0.494 \\ f_2 = 0.500 \\ f_3 = 0.818 \end{bmatrix} \text{Hz}, \quad \underset{\sim}{\phi} = 10^{-3} \begin{bmatrix} -1.211 & 1.617 & 0.143 \\ 1.606 & 1.220 & -0.190 \\ 0.238 & -2.15 \times 10^{-15} & 2.011 \end{bmatrix} \tag{5}$$

The modal centers of velocity are located as indicated in Fig. 1a, Eq. (4). Note, the dominating rotational mode number 3 is excited in general by the seismic forcing since C_{v3} is distinct from the center of mass C_M, its modal participation factor does not vanish, contrary to the purely rotational mode of a perfectly symmetric building.

3 Design of the novel base isolation element and its stability

The novel base isolation element as proposed by Khalid [8] substitutes the "classical" reinforced rubber element and is sketched in Fig. 2a with dimensions indicated. With respect to the proper selection of the linear elastic helical steel spring, we note the design equations for its vertical (axial) and horizontal (shear) stiffness, and their ratio to be maximized within proper design limits, where n_t is the number of turns; E, the modulus of elasticity; and ν, Poissons' ratio, see for example, Ziegler [18], p. 385 and Parkus [19], p. 288,

$$k_{1v} = Ed\frac{(d/2D)^3}{2\,(1+\nu)\,n_t}, \; k_{1h} = Ed\frac{(d/2D)^3}{n_t\left[1+(4/3)\,(2+\nu)\,(l/D)^2\right]}$$
$$\lambda_{vh} = \frac{k_{1v}}{k_{1h}} = \frac{1+(4/3)\,(2+\nu)\,(l/D)^2}{2\,(1+\nu)} \Rightarrow \max \tag{6}$$

When considering the static stability of the pivoted upright-pendulum supported by the horizontal stiffness of the helical spring, Fig. 2a, only a fraction of the dead weight of the building (well below the critical buckling load $k_{1h}l$, [18], p. 519) is carried by the column and thus axial prestressing $k_{1v}l\,(l_0/l-1) > 0$ of the spring

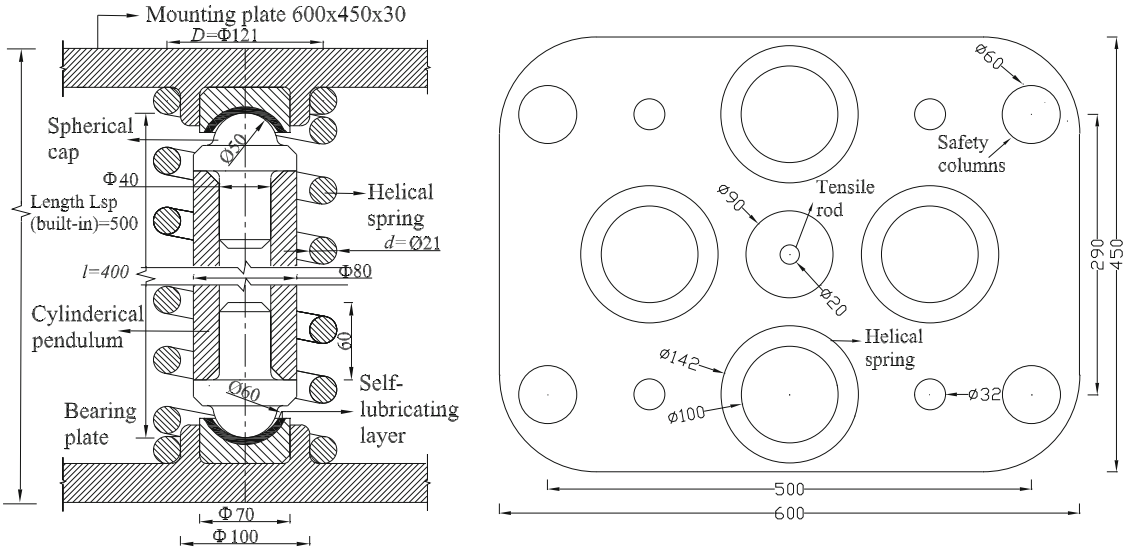

Fig. 2 Novel base isolation element consisting of an axially prestressed helical steel spring and a pinned-pinned column in spherical bearings lined with self-lubricating porous bronze layers (indicated by thickened *black lines*), Khalid [8]. **b** Schematic plan of a 4-spring-pendulum unit with 4 safety steel columns (Φ60) with axial clearance limiting the tilting angle $|\phi| \leq 33°$

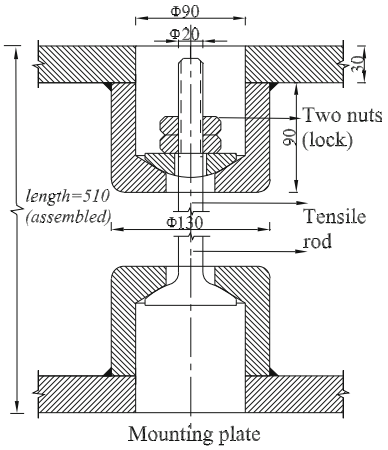

Fig. 3 Central tensile-rod arrangement for the axial compression of helical springs in the assembly stage, dimensions as of Fig. 2b, Khalid [8]

is required. For a number of N base isolation elements, a first condition follows at once from the ratio of the total building weight to the resulting buckling force,

$$m_S g/Nk_{1h}l = \lambda + \lambda_{vh}\,(l_0/l - 1)\,, \quad 0 < \lambda < 1 \tag{7}$$

The load factor λ of the upright pendulum used to define the required axial pre-stress of the spring must be positive to assure a compressive axial force, and it is quantified when considering the quasi-static action of the maximum vertical ground acceleration, commonly set proportional to the horizontal component, $a_{gv} = \lambda_x a_g$, λ_x depends also on the site soil conditions. Equation (7) extends to

$$m_S g\left(1 \pm a_{gv}/g\right)/Nk_{1h}l = \lambda_{gv} + \lambda_{vh}\,(l_0/l - 1)\,, \quad 0 \le \lambda_{gv} < 1 \tag{8}$$

when λ_{gv} denotes the dynamic load factor of the upright pendulum. Subtracting Eq. (7) from Eq. (8) yields the universal and crucial condition that must hold for both up- and downward ground motion,

$$\pm\, a_{gv} = \frac{Nk_{1h}l}{m_S}\left(\lambda_{gv} - \lambda\right) \tag{9}$$

With λ_{gv} considered either close to one, say $\lambda_{gv} = 0.98$ or zero, the static load factor becomes $\lambda = 0.98/2 = 0.49$ and, when substituted in Eq. (8) yields the required prestress, expressed by the shortening $(l_0 - l)$of the helical spring, [8]. Further, considering the equal sign in Eq. (2) and substituting the resulting value$Nk_{1h}/m_S = \pi^2$ in Eq. (9) conservatively estimates the maximum tolerable vertical ground acceleration in terms of the length of the upright pendulum and prestressed coil spring,

$$\max a_{gv}/g = \lambda l\pi^2/g = 0.493l \tag{10}$$

In the case, when higher values of the vertical ground acceleration apply at the site, purely kinematical considerations of the downward ground movement during the short time interval when the acceleration exceeds the limit given in Eq. (10) render a quite relaxed conservative estimate. For instance, putting $l = 400$ mm, Eq. (10) determines the lower conservative estimate, $\max a_{gv} = 0.2g$. However, assigning, for example, the El Centro seismogram scaled to $\max a_{gv} = 0.32g$, (firm soil is considered), that is, putting $\lambda_x = 1$, Khalid [8] reported no loss of contact of the upright pendulum from its spherical bearings to occur. However, to ensure contact stability even in the maximum allowed tilted configuration, the expansion of the isolation element is limited by a properly designed tensile-rod arrangement, sketched in Fig. 3, that also serves the purpose of prestressing before the assembled element is built-in.

The static stability of the isolation element, even including the post-buckling regime with tilting angle ϕ, is guaranteed by Dirichlets stability criterion, Ziegler [18], p. 517, when applied to the potential function, single dead-weight load F_{1v},

$$E_p = U + W = l^2 k_{1h}\left\{\frac{1}{2}\,(1 - \lambda_{vh})\sin^2\varphi + \lambda_{vh}\,(1 - \cos\varphi)\right\} - F_{1v}l\,(1 - \cos\phi) \tag{11}$$

A stable bifurcation requires both, the admissible dead-weight load to be smaller than the critical load $k_{1h}l$ and the axial (compressive) stiffness of the helical spring to be larger than its horizontal (shear) stiffness,

$$\lambda = F_{1v}/k_{1h}l < 1, \lambda_{vh} = k_{1v}/k_{1h} > 1 \tag{12}$$

This latter condition supports the functional requirement for the isolation element to maximize the ratio of vertical to horizontal stiffness of the helical spring, as such matching as close as possible that of the classical reinforced rubber element.

Four SP elements are assembled to act in parallel, termed as the helical spring-pendulum (SP) unit (weight less than 50 kg) for the convenience of mounting the base isolation elements in the continuous foundation of a building, schematically sketched in Fig. 2b. Thus, the building rests on a number $N/4$ of such assembled SP-units, to be arranged in an equidistant manner along the perimeters in-between the rigid strip foundations of the building (e.g., a masonry construction). The provision of safety columns is a standard strategy to support the building in case of any failure or mishap of the isolation units. Thus, for the exemplarily considered single-storey asymmetric building four safety steel columns with 70-mm axial clearance, corresponding to the maximum allowed tilting angle of $|\phi| = 33°$, (based on the response of the building under El Centro 1940 seismogram scaled to 0.32 g). Any soil-structure interaction is neglected on firm soil. For example, also rocking, each assembled SP-unit limits the further downward movement of the building. Contrary to the classical base isolation element based on reinforced rubber sheets, with a high vertical stiffness that allows even a rocking at foundation level, our proposed novel design excludes any rotational stiffness due to the guided motion by the "upright pendulum" in contact. The latter, made of steel, can be assumed to be rigid.

A sufficient axial compression of the springs in the assembled stage is achieved by means of a tensile-rod arrangement at the center of the unit, Fig. 2b. The working of this arrangement can be comprehended from the Fig. 3: The tightening of the nut driven a certain allowed distance (limited length of the threads) on the tensile-rod creates tensile forces in the rod thus brings the mounting plates closer by compressing the four symmetrically arranged helical springs as required, namely just to keep the upright-pendulum in contact with its spherical bearings. However, in the built-in stage, the rod becomes loose when the portion of the building's weight further compresses the helical springs axially and it remains loose when the pendulum is tilted during the action of the earthquake.

However, if such an asymmetric building has a skeletal structure, its weight is transmitted to the ground by means of main columns, and the same design of the isolation unit may serve the purpose with a proper concentration of the required number of isolation elements per column. Thus, for example, if the weight of the same building as considered above is supported on twenty columns, a total of twenty isolation units each having twelve isolation elements of one and the same design are required to be combined in parallel action. The arrangement of the twelve isolation elements on two concentric circles, say of diameter 400 and 600 mm, respectively, with the upper and lower mounting plates of diameter 800 mm, is illustrated in Fig. 4. Axial compression of the twelve helical springs in the assembled SP-unit is achieved by means of a centrally built-in tensile-rod (say of size M-40), a design analogous to that shown in Fig. 2b. The safety columns, however, are not included in such a modified SP-unit but are separately arranged outside of the unit,—likewise to the classical standard constructions in base isolation with rubber bearings.

The dimensions of the isolation element applied to the illustrative single story building, Fig. 2a, are listed in Table 1.

The separately designed novel sliding elements, subsequently described in Section 4, can be put between the shear walls of the skeletal building and their strip foundations since the horizontal forces of these elements to be transmitted to the ground are rather small—for the classical system, see again Bachmann [7].

4 Sliding element without continuous energy dissipation

The novel base isolation system is complemented by separately acting sliding elements that provide limited static friction, however, without continuous energy dissipation in abrasive dry friction. For design details see again Khalid [8]. For the single-storey asymmetric building under consideration where the damping is supplied by means of TLCGDs, the purpose of the sliding elements is just to resist the loads by wind gusts and small seismic disturbances, for example, of traffic origin. Thus, for example, the averaged stagnation pressure of a wind gust (average wind speed assumed as $v_w = 15.5\text{m/s}$), $p_{av} = \rho_a v_w^2/2 = 150\text{N/m}^2$, renders the resulting horizontal wind force, say acting on the larger face of the building to be $F_w = 9\text{kN}$. A single novel sliding element, as proposed in [8], consists of a circular steel plate of diameter $D_{ls} = 200\,\text{mm}$ coated with a 5-mm

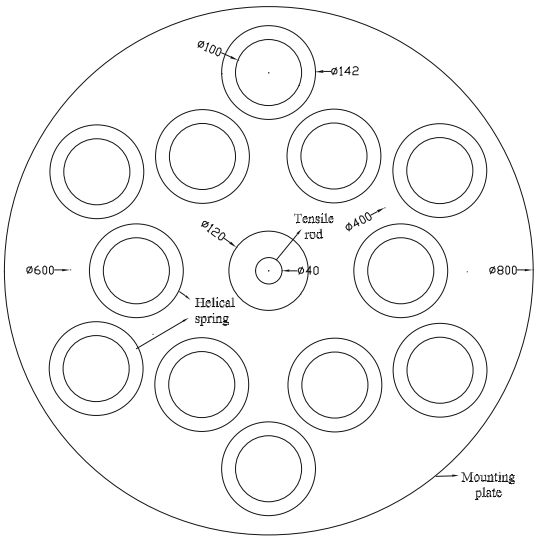

Fig. 4 Spring-pendulum (SP) unit in skeletal building, having 12 isolation elements arranged in two concentric circles; with a tensile-rod in central position acting during the assembly stage, cf. Fig. 2b. Safety columns placed outside of the unit are not shown [8]

Table 1 Key parameters of a single base isolation (SP) element, $N = 240$, [11]

Parameters	Values
Horizontal stiffness of helical spring, k_{1h} (N/mm), Eq. (2)	10.02
Length of axially prestressed helical spring, l (mm)	400
Number of active turns/coils of helical spring, n_t	8
Outer spring diameter, D_e (mm)	142
Diameter of the wire of helical spring, d (mm), Eq. (6)	21
Vertical stiffness of helical spring, k_{1v} (N/mm), Eq. (6)	130.95
Vertical to horizontal stiffness ratio, $\lambda_{vh} = k_{1v}/k_{1h}$, Eq. (6)	13.06
Mean diameter of spring, $D = D_e - d$ (mm)	121
Spring index, $C = D/d$	5.8
Pre-compression, δ_v (mm), Eq. (7) for load factor $\lambda = 0.49$	61
Free spring length, $l_0 = l + \delta_v$ (mm)	461
Critical buckling load, $F_{1v,cr} = k_{1h} l$ (kN), $\lambda_c = 1$	4.01
Force in upright-pendulum, $F_{1v} = \lambda F_{1v,cr}$, $\lambda = 0.49$ (kN)	1.96
Force in spring due to axial pre-stress, $F_{1r} = k_{1v}(l_0 - l)$ (kN)	8.00
Vertical deflection at $\lvert\varphi\rvert = 33°$, $\delta_{1v} = l(1 - \cos\phi)$ (mm)	70
Length of spring, when tilted, $l_1 = l - \delta_{1v}$ (mm)	330
Allowance before solid, $l_a = l_1 - l_s$, (mm), $l_s = n_t d = 168$ mm	162

bronze layer in contact with another circular steel plate of sufficiently larger diameter, say $D_{us} = 680$ mm, connected to the upper foundation beam of the building so as to establish a bronze–steel interface between upper and lower sliding plates. Therefore, considering the coefficient of static friction at the interface (bronze–steel contact) $\mu = 0.2$, the resulting normal force $R_v = F_w/\mu = 45$ kN dictates the total number of sliding elements required to be placed in-between the aseismic foundation. The static contact at the bronze–steel interface is maintained at rest by a pre-compressed conical steel spring with a proper axial displacement, say of $\delta_v = 60$ mm. Choosing the number $N_s = 8$ of such sliding elements to be arranged as illustrated in Fig. 2a, we get the required vertical stiffness of one conical spring,

$$k_{1v}\delta_v = R_v/N_s, k_{1v} = 93.75\,\text{N/mm} \tag{13}$$

The conical spring is adopted to take the advantage of its less solid height and is designed as a linear spring with constant spring rate whereas the pitch is variable so that all coils come to touch each other at the same instant when pressed to solid. Thus, the averaged diameter D of the conical spring is to be substituted in the first expression in Eq. (6). The design and other key parameters of the conical spring are listed in Table 2.

Table 2 Parameters of conical spring and the lever in a sliding element [8]

Parameters	Values
Number of active turns/coils of conical spring, n_t	4
Axial stiffness of conical spring, k_{1v} (N/mm), Eq. (6)	93.75
Diameter of the wire of conical spring, d (mm)	25
Average diameter of conical spring, D (mm), Eq. (6)	220
Spring index, $C = D/d$	8.68
Required full deflection of the spring (mm)	218
Pre-compression, δ_v (mm)	60
Force under pre-compression $F_{1r} = k_{1v}\delta_v$ (kN)	5.63
Free length of conical spring, $l_0 = l_s + \delta_{1v} + \delta_v + l_a$, (mm)	325
$l_a = 22$ mm; allowance before solid, $l_s = d = 25$ mm	
Length of the axially compressed conical spring, $l = l_0 - \delta_v$ (mm)	265
Length of lever amplifying the vertical motion, L_l (mm)	720
Cross-sectional area of lever, $A_l = (2b_l + 2h_l)t_l (\text{mm}^2)$ (with a thin-walled sandwich cross-section $b_l = 120,\ h_l = 60,\ t_l = 5$ mm)	1,800
Critical force in lever, $F_{l,cr} = k_{1v}L_l$ (kN)	67.5
Normal stress, $\sigma_l = F_{l,cr}/A_l$ (MPa)	37.5
Virtual static friction coefficient, $\mu = F_{l,cr}/F_{1r}$	12

In the strong motion phase of an earthquake, the foundation beams of the rigid asymmetric building experience a relative horizontal motion associated with the vertical downward movement. It is also desired that the sliding elements should not offer continuous friction by the abrasive contact (i.e., no continuous frictional energy dissipation in this horizontal movement) that can be achieved if the contact at the bronze–steel interface is released. For this purpose, a lever system consisting of three mechanical levers arranged at 120° apart as illustrated in Fig. 4 is proposed to magnify the vertical motion of the building at their tips when contacting the lower sliding plate. Levers of sufficient length, with thin-walled sandwich cross-sections, scaled sketch in Fig. 4, dimensions listed in Table 2, are designed to serve the purpose. One end of the lever is simply supported on the lower foundation beam whereas the opposite end is connected to the extended flanges of the lower sliding plate by means of a bolt, moveable axially in a proper slit, see again Fig. 4. Thus, the wind forces in static friction are transmitted to the ground mainly by compressive axial forces in the levers (metal contact of the bolt in the slit). The pre-stressed neoprene spring (a bar of about 200 mm length) within the hollow lever is pre-tensioned against the bolt of the bearing of the lower sliding plate.

A ring-flange at the periphery of the upper sliding plate (moving with the building) contains densely packed ball bearings and is attached to the upper foundation beam of the building such that the ball bearings just loosely touch the levers under some local admissible clearance. The action of the lever is simple and can be grasped for instance: during any horizontal movement, the ball bearing slides on the lever and the associated vertical downward movement simply push the lever down as required. Thus, the tip of the lever connected to the lower sliding plate forces it to an amplified downward displacement by further compressing the conical spring, and hence, the contact at the bronze–steel interface is released. The bolt in the bearing at the lower sliding plate moves down vertically; consequently, it slides in the slit provided in the lever's cross-sectional sidewalls, Fig. 5.

5 Effective modal damping by the TLCGD

Adding damping elements that have no moving mechanical parts completes the novel base isolation system. Hochrainer, see again [13], has invented the gas-spring effect acting in parallel connection to the gravitational restoring force of the classical TLCD, Fig. 1b. It renders an additional parameter for convenient frequency tuning of the TLCGD. The equation of the relative fluid flow in the symmetrically designed TLCGD, when installed in the basement of the building and with the trace oriented in a general direction, say angle γ, is derived by integrating along the instant relative streamline to render a generalized non-stationary Bernoulli equation, [18], page 497, considering a moving frame. Derivations in connection with the effective modal damping of multipurpose, asymmetric buildings are worked out in [17]. The TLCGD consists of a U- or V-shaped piping system partially filled with water, when oscillating with a common liquid stroke, $u_1 = u_2 = u(t)$, Fig. 1b. For the TLCGD tuned with respect to the structural mode number j, the respective parameters are understood to carry this mode number [8],

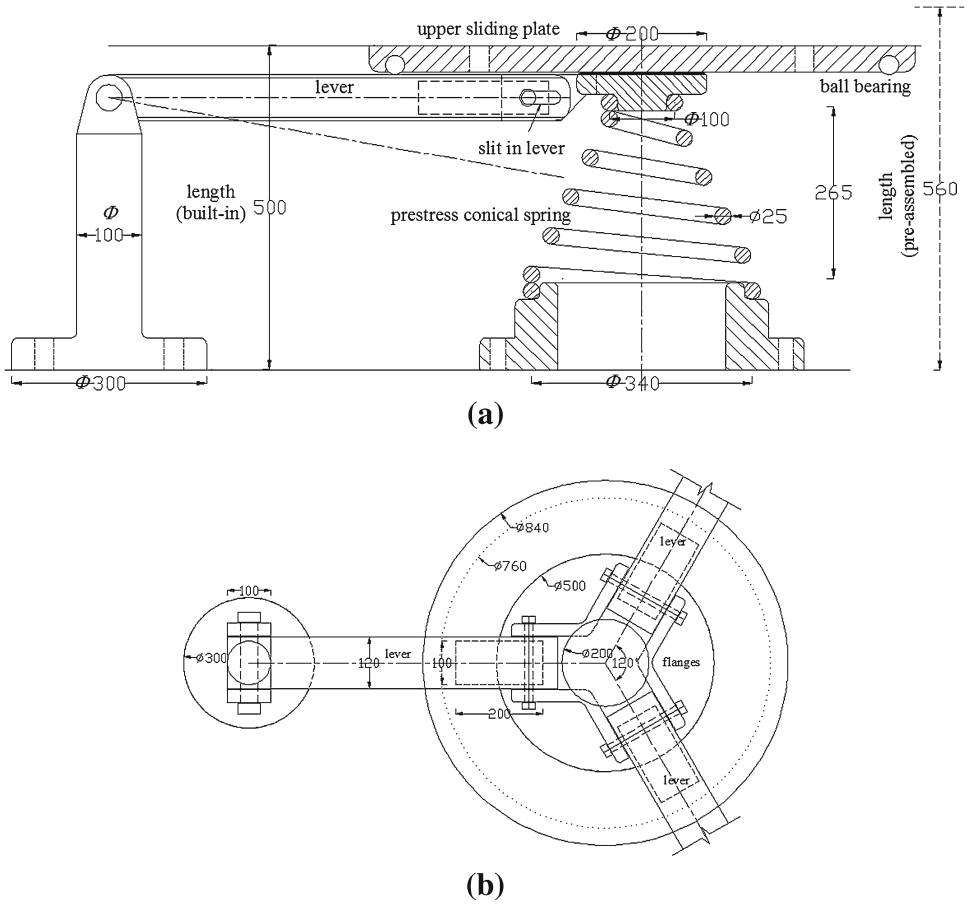

Fig. 5 Scaled sketch of a single sliding element providing static friction, but without continuous energy dissipation. **a** Elevation with conical spring and the lever system shown. **b** Plan, three levers, amplifying the vertical motion of the lower sliding plate is illustrated [8]

$$\ddot{u}_j + 2\zeta_{Aj}\omega_{Aj}\dot{u}_j + \omega_{Aj}^2 u_j = -\kappa_j \left\{ \begin{array}{l} a_g \cos\left(\alpha - \gamma_j\right) + \left[\ddot{v}_M - \ddot{u}_T \frac{z_{Aj} - z_M}{r_S}\right] \cos\gamma_j \\ + \left[\ddot{w}_M + \ddot{u}_T \frac{y_{Aj} - y_M}{r_S}\right] \sin\gamma_j \end{array} \right\} \tag{14}$$

$$\kappa = (B + 2H\cos\beta)/L_{\text{eff}},\ L_{\text{eff}} = (A_H/A_B)\, B + 2H$$

Considering the absorber damping to be sufficiently high, parametric excitation by both, the vertical component of ground acceleration and the rotation about the vertical x-axis, becomes negligible and the simplified Eq. (14) results. The severe case of vertical ground acceleration requires (the critical double frequency time-harmonic forcing is considered, see [20] for a detailed analysis)

$$\zeta_A > \zeta_{A,0} = \frac{a_{gv}/g}{4\,(1 + h_0/H_a \sin\beta)} \tag{15}$$

The viscous damping in Eq. (14) represents the equivalently linearized, experimentally observed mean turbulent damping $\delta_L\,|\dot{u}|\,\dot{u}$: Hence, the viscous coefficient turns out to be proportional to the fluid stroke, $\zeta_A = (4/3\pi)\,\delta_L \max|u|$, [13]. The linearized Eq. (14) enters the modal tuning process that, by analogy, in a first step, can be based on the Den Hartog optimization of the equivalent TMD; see again [13] for details. Thus ζ_A is inserted with its optimal value. The absorber frequency in Eq. (14) takes on an optimal value (result of frequency tuning) and can be set equal to the natural frequency of small vibrations of a mathematical pendulum of length L_0, to render a design formula in its most convenient form to define the required equilibrium gas pressure, $np_0 = \rho g h_0$, $1 \le n \le 1.4$, in relation to the size of the one-sided gas volume $V_a = A_H H_a$ in each limb as required by the condition for linearized gas compression, $\max|u| \le H_a/3$, (mode number j understood accordingly),

$$f_A = \frac{\omega_A}{2\pi} = \sqrt{\frac{g/\pi^2}{4L_0}}(\text{Hz}),\ L_0 = L_{\text{eff}}/2\,(\sin\beta + h_0/H_a)$$
$$\Rightarrow h_0/H_a = L_{\text{eff}}/2L_0 - \sin\beta,\ h_0 = np_0/\rho g \tag{16}$$

For the application of the piston theory, that is, to keep the fluid–gas interface intact, a severe limit on the maximum allowable (relative) fluid speed has to be observed, limiting the absorber frequency for a given maximum stroke by about, see [21],

$$\max|u|\,2\pi f_A \le 12\ \text{m/s} \tag{17}$$

5.1 Control forces of TLCGD acting in the basement of the base isolated rigid building, number j understood

Considering the absolute horizontal acceleration of the center of mass C_f of the displaced fluid column, conservation of both, momentum and angular momentum renders the generalized control force components as listed in their linearized form (just to enter the approximate substructure synthesis with Eq. (1)) and the moment (when referred to the center of mass of the building C_M): the details of derivations are given in [17],

$$\begin{aligned}
F_y &= m_f\left[a_g\cos\alpha + \ddot{v}_M - \ddot{u}_T(z_A - z_M)/r_x\right] + \bar{\kappa}m_f\ddot{u}\cos\gamma, \quad \bar{\kappa} = \kappa L_{\text{eff}}/L_1\\
F_z &= m_f\left[a_g\sin\alpha + \ddot{w}_M + \ddot{u}_T(y_A - y_M)/r_x\right] + \bar{\kappa}m_f\ddot{u}\sin\gamma, \quad m_f = \rho A_H L_1\\
M_x &= m_f\bar{\kappa}_3\ddot{u}_T H^2/r_x - F_y\,(z_A - z_M) + F_z\,(y_A - y_M)\\
\bar{\kappa} &= \{[1 + (A_B/3A_H)\,(B/2H)]\,(B/2H) + [1 + (2H/3B)]\cos\beta\}\,(B/L_1)
\end{aligned} \tag{18}$$

5.2 Modal tuning

Equation (1) is modally expanded, $\vec{x} = \sum_{j=1}^{3} q_j\,(t)\vec{\phi}_j$, however, the modal coupling present in the generalized control forces (18) is neglected in a first step for the sake of modal tuning of the selected TLCGD by means of a transformation of Den Hartog's optimization formulas in the design stage, [13]. Considering subsequently this modal coupling in the fine-tuning process using the readily available optimization tools in state space makes the required corrections. The approximating result with Eq. (14) substituted for the isolated j-th mode renders a two DOF coupled system $\left[q_j\ u_j\right]^T$, and the extremely light damping in the base isolation is commonly assumed to be constant, $\zeta_{Sj} = \zeta_S \approx 0.05$ or even less, [8].

Thus, the isolated generalized single-degree mode combines with the TLCGD equation in the approximating matrix equation to form the coupled 2 DOF system,

$$\begin{bmatrix} 1+\mu_j & \bar{\kappa}_j\mu_{fj}V_{\gamma j} \\ \kappa_j V_{\gamma j} & 1 \end{bmatrix}\begin{bmatrix}\ddot{q}_j \\ \ddot{u}_j\end{bmatrix} + \begin{bmatrix} 2\zeta_{Sj}\omega_{Sj} & 0 \\ 0 & 2\zeta_{Aj}\omega_{Aj}\end{bmatrix}\begin{bmatrix}\dot{q}_j \\ \dot{u}_j\end{bmatrix} + \begin{bmatrix}\omega_{Sj}^2 & 0 \\ 0 & \omega_{Aj}^2\end{bmatrix}\begin{bmatrix} q_j \\ u_j\end{bmatrix} = -\begin{bmatrix} L_j \\ \kappa_j\cos(\alpha - \gamma_j)\end{bmatrix}a_g \tag{19}$$

$$\begin{aligned}
&\mu_{fj} = m_{fj}/m_j,\ \mu_j = \mu_{fj}V_j^2,\ V_j^2 = V_j^{*2} + \bar{\kappa}_{Tj}\left(H_j\phi_{j3}/r_x\right)^2,\quad V_j^{*2} = v_{A,j}^2 + w_{A,j}^2\\
&v_{A,j} = \phi_{j1} - \phi_{j3}\left(z_{Aj} - z_M\right)/r_x,\ w_{A,j} = \phi_{j2} + \phi_{j3}\left(y_{Aj} - y_M\right)/r_x,\quad V_{\gamma j} = v_{A,j}\cos\gamma_j + w_{A,j}\sin\gamma_j\\
&L_j = L_{yj}\cos\alpha + L_{zj}\sin\alpha,\ L_{yj}^{=}\mu_{Sj}\phi_{j1} + \mu_{fj}v_{A,j},\quad L_{zj} = \mu_{Sj}\phi_{j1} + \mu_{fj}w_{A,j}
\end{aligned}$$

The transformation of the optimal equivalent TMD parameter, [12], requiring $\omega_{Aj}^* = \omega_{Aj}$, $\zeta_{Aj}^* = \zeta_{Aj}$, is deduced by comparing Eq. (19) with the set of equations considering the TMD action, see [13] and [21] for details, and a star refers to the TMD parameters of the spring-(point-) mass-dashpot type; the TMD modal mass ratio turns out somewhat lower than that of the equivalent TLCGD,

$$\mu_j^* = \mu_j \frac{\kappa_j \bar{\kappa}_j \left(V_j^*/V_j\right)^2}{1 + \mu_j \left(1 - \kappa_j \bar{\kappa}_j \left(V_j^*/V_j\right)^2\right)} < \mu_j,$$
$$\delta_{j\text{opt}} = \frac{f_{Aj,\text{opt}}}{f_{Sj}} = \frac{\delta_{j\text{opt}}^*}{\sqrt{1 + \mu_j \left[1 - \kappa\bar{\kappa} \left(V_j^*/V_j\right)^2\right]}}, \zeta_{Aj} = \zeta_{Aj}^* \tag{20}$$

The dead fluid mass is apparent in the denominator in Eq. (20). The Den Hartog optimal formulas of TMD for minimum total acceleration are, [12] and, for that optimization see [22],

$$\delta_{\text{opt}}^* = \frac{1}{1 + \mu^*}, \zeta_{\text{opt}}^* = \sqrt{\frac{3\mu^*}{8\,(1 + \mu^*)}} \tag{21}$$

5.3 Fine-tuning of the coupled set of three TLCGDs in state space

Full modal expansion of Eqs. (1), (14) and (18), substituted, yields six coupled, still approximating modal equations. Keeping the generalized coordinates, the 12×1 state vector $\vec{z}$ is defined by the first-order set of differential equations,

$$\dot{\vec{z}}\,(t) = \left(\underset{\sim}{A} + \underset{\sim}{B}\underset{\sim}{R}\right)\vec{z}\,(t) + \underset{\sim}{E}_g\,\vec{a}_g(t), \vec{z}^T = \left[\vec{q}^T\,\vec{u}^T\,\dot{\vec{q}}^T\,\dot{\vec{u}}^T\right] \tag{22}$$

where the system matrix $\underset{\sim}{A} + \underset{\sim}{B}\underset{\sim}{R}$ is kept separated to explicitly handle the TLCGD parameter for the sake of fine-tuning. In case, the cross-sectional area of the piping system turns out to be too large, and the size of the system is extended to account for smaller TLCGD units in parallel action to assure a one-dimensional fluid flow or for design reasons related to space limitations within the basement. In that case, the absorber frequencies and damping coefficients of the fluid flow in the smaller units are subjected to fine-tuning too, see 4.3.1, and the stroke of the TLCGD number j in Eq. (22) becomes a vector sampling the individual strokes $\vec{u}_j^T = \left[u_{j1}\ u_{j2} \ldots\right]$.

Thus, for this sake, a time-harmonic ground acceleration is considered, and the complex solution of the state hyper vector becomes

$$\vec{z}_0\,(\alpha, \omega) = \left[i\omega\underset{\sim}{I} - \left(\underset{\sim}{A} + \underset{\sim}{B}\underset{\sim}{R}\right)\right]^{-1} \underset{\sim}{E}_g\,\vec{e}_g a_0, \vec{z}_{0j} = \left[q_{0j}\ u_{0j}\ i\omega q_{0j}\ i\omega u_{0j}\right]^T \tag{23}$$

The optimal parameters, contained in the hyper matrix $\underset{\sim}{\rightarrow}\ R$, are calculated by minimizing a performance index, for example, considering the minimum of the area under the frequency response function of the main system; thus, the state vector of the main system, expressed in generalized modal coordinates $\vec{z}_S = \left[\vec{q}\ \dot{\vec{q}}\right]$, is considered to fully transfer the coupling to the combined action of several TLCGDs and in its time reduced form—possibly with a positive semi-definite weighing (diagonal) matrix $\underset{\sim}{S}$ chosen to pronounce, for example, the amplitudes of the generalized coordinates, say ten times over the generalized velocities, Khalid [8],

$$J = \int_{-\infty}^{\infty} \vec{z}_{0S}^T(\omega)\underset{\sim}{S}\vec{z}_{0S}(\omega)\mathrm{d}\omega = 2\pi \left[\underset{\sim}{E}_g\,\vec{e}_g a_0\right]^T \underset{\sim}{P}\,\underset{\sim}{E}_g\,\vec{e}_g a_0 \rightarrow \min \tag{24}$$

$\underset{\sim}{P}$ is consequently the solution of the algebraic Lyapunov matrix equation [23],

$$\left(\underset{\sim}{A} + \underset{\sim}{B}\underset{\sim}{R}\right)^T \underset{\sim}{P} + \underset{\sim}{P}\left(\underset{\sim}{A} + \underset{\sim}{B}\underset{\sim}{R}\right) = -\underset{\sim}{S} \tag{25}$$

Although derived for harmonic excitation, the state space optimization can also be interpreted in terms of stochastic quantities. Assuming the ground excitation to be a stationary random white noise process, the structural vibration response can be characterized by a random process with zero mean and a covariance matrix given

Table 3 Parameters of diagonal TLCGD1 and 2, and z-parallel TLCGD3 [8]

Description	1	2	3
Three TLCGDs, their orientation and position	$\gamma_1 = 115°$	$\gamma_2 = 45° A(-1.9, 0)$	$\gamma_3 = 90° A(-6, 0)$
Mass of water in TLCGD, m_f (kg)	5000	4200	500
Modal mass ratio,μ_j (%), $m_j = 1$, Eq. (19)	2.25	1.72	0.6
Horizontal length of liquid column, B (m)	8.4	10.8	8
Vertical height of the liquid column, H (m)	1.65	1.75	0.5
Effective length, $L_{\text{eff}} = B + 2H$ (m)	11.7	14.3	9.0
B/L_{eff}	0.718	0.755	0.889
Inner diameter, circular TLCGD pipe, (mm)	737	612	266
Geometry factor, $\kappa = \bar{\kappa}$, Eq. (14)	0.72	0.755	0.889
Optimal frequency ratio, δ_{opt}, Eq. (20)	0.983	0.987	0.995
Optimal absorber frequency, $f_{A,\text{opt}}$ (Hz)	0.486	0.493	0.814
Optimal damping coeff., $\zeta_{Aj} = \zeta_{Aj}^*$ (%)	6.51	6.02	3.97
Math. pendulum length, L_0 (m), Eq. (16)	1.053	1.021	0.375
$h_0/H_a = L_{\text{eff}}/2L_0 - \sin\beta$	4.557	6.003	11.004
"Pressure head", $h_0 = np_0/\rho g, n = 1$, (m)	13.76	15.80	12.232
Gas volume, $V_0 = A_H H_a (\text{m}^3)$	1.291	0.773	0.062
Dead fluid mass (kg), apparent in Eq.(20)	2436	1804	105

by $\underset{\sim}{P}$, see again [23]. In that case the covariance matrix is an important response measure, since the standard deviation of the states is given by diagonal elements. The minimum of the performance index J is numerically searched. The unconstrained quadratic optimization with initial tuning parameter obtained by the transformed Den Hartog optimal parameter, for example, is quickly performed with the function *fminsearch* of the Matlab [16] optimization toolbox, see again [13] and [17] for details. The parameter optimization of Eq. (24) may also include uncertainty of the building mass and uncertainty of the base isolation stiffness by generalizing the performance criterion. If, for example, the extreme variations in the mass and stiffness distribution (including aging effects) are estimated in relation to the ideal base isolated structure, minimizing the sum of the associated performance indices can be performed to adapt the optimal TLCGD parameter,

$$J = J_{A_r} + J_{A_{r\,\min}} + J_{A_{r\,\max}} \to \min \tag{26}$$

where $J_{A_r} = J$ of the regular structure, Eq. (24)

The fluid mass (of water) in the three TLCGDs considered in [8] is chosen $m_{f1} = 5,000\,\text{kg}$, $m_{f2} = 4,200\,\text{kg}$ and $m_{f3} = 1,000\,\text{kg}$. Since the structural modal damping of such a base-isolated building is extremely low even with linearized frictional damping of the novel sliding elements included, it is assumed constant 0.5 % in each mode. The dimensions of the TLCGDs and other resulting key parameters at corresponding modally critical angles of incidence of the seismic excitation $\alpha_{cr} = 125, 40, 125°$ are collected in Table 3.

5.3.1 State space equations of an isolated single structural mode combined with small units of the TLCGD

Isolating the structural mode number j and splitting the associated TLCGD into say three smaller units in parallel action yields the set of eight state equations of first order. In the illustrative example such a division is recommended for the TLCGDs numbered $j = 1$ and 2. The state vector components are chosen, $z_1 = q_j$ together with the individual fluid strokes in the smaller units $z_2 = u_{jn_1}$, $z_3 = u_{jn_2}$, $z_4 = u_{jn_3}$, and the extended Eq. (19) is considered with fluid mass equivalently distributed and by keeping the effective length L_{eff} of the fluid column unchanged,

$$\dot{z}_1 = z_5, \dot{z}_2 = z_6, \dot{z}_3 = z_7, \dot{z}_4 = z_8 \tag{27}$$

$$\begin{aligned} \dot{z}_5 = &-\bar{\eta}_{\gamma j} \\ &\times \left\{ \begin{array}{l} \left(\omega_{Sj}^2 z_1 + 2\zeta_{Sj}\omega_{Sj} z_5\right) - \bar{\kappa}_j V_{\gamma j} \frac{\mu_{fj}}{3} \sum_{n_i=1}^{3} \left(\omega_{Ajn_i}^2 z_{n_i+1} + 2\zeta_{Ajn_i}\omega_{Ajn_i} z_{n_i+5}\right) \\ + \left[L_j - \mu_{fj}\kappa_j\bar{\kappa}_j V_{\gamma j}\cos\left(\alpha - \gamma_j\right)\right] a_g \end{array} \right\} \end{aligned} \tag{28}$$

$$\bar{\eta}_{\gamma j} = \left[1 + \mu_{fj}\left(V_j^2 - \kappa_j\bar{\kappa}_j V_{\gamma j}^2\right)\right]^{-1}, \quad j = 1 \text{ or } 2.$$

Subsequently the substitution of $\dot{z}_5$ as given in Eq. (28) is understood,

$$\begin{aligned}
\dot{z}_6 &= -\omega_{Ajn_1}^2 z_2 - 2\zeta_{Ajn_1}\omega_{Ajn_1} z_6 - \kappa_j V_{\gamma j}\dot{z}_5 - \kappa_j a_g \cos\left(\alpha - \gamma_j\right) \\
\dot{z}_7 &= -\omega_{Ajn_1}^2 z_3 - 2\zeta_{Ajn_1}\omega_{Ajn_1} z_7 - \kappa_j V_{\gamma j}\dot{z}_5 - \kappa_j a_g \cos\left(\alpha - \gamma_j\right) \\
\dot{z}_8 &= -\omega_{Ajn_1}^2 z_4 - 2\zeta_{Ajn_1}\omega_{Ajn_1} z_8 - \kappa_j V_{\gamma j}\dot{z}_5 - \kappa_j a_g \cos\left(\alpha - \gamma_j\right)
\end{aligned} \tag{29}$$

The time-harmonic solution $\vec{z}_{0S} = q_{0j}\left[\,1\;i\omega\,\right]^T$ is consequently substituted into Eq. (24) to render the parameter of the individual TLCGD-units optimal. In a second step, the coupling of all absorbers can be considered resulting in a slight change of the optimal TLCGD parameter.

5.4 Dimensioning of the TLCGD piping system

For the sake of simplicity, a straight circular cylindrical pipe with radius r and wall thickness $t \ll r$ is considered for estimating its dimensions. The membrane hoop stress σ_h due to the internal gauge pressure p_g is determined by the pressure-vessel formula, for example, see [18], p. 91, the admissible tensile stress of steel is noted,

$$\sigma_h = p_g r/t \leq \sigma_a = 15\,\mathrm{N/mm^2} \tag{30}$$

In the compression phase, the maximum possible stroke $\max|u| = H_a/3$ is considered for safety reasons to render for an adiabatic process the maximum gauge pressure, see [8] for details,

$$p_{g\,\max} = 1.76 p_0 + \rho g\,(H + H_a/3) - p_{atm} \tag{31}$$

In the extreme expansion phase, the minimum gauge pressure should remain positive (to avoid a compressive hoop stress) and becomes, see again [11],

$$p_{g\,\min} = 0.67 p_0 - p_{atm} > 0 \tag{32}$$

In practice, however, for that extreme liquid stroke, negative gauge pressures, that is, external pressure loads, are possibly acceptable if far below the critical buckling pressure, Young [24], p. 690,

$$p_{cr} = \frac{E}{4\left(1-\nu^2\right)}\,(t/r)^3 \tag{33}$$

A wall thickness of $t = 5\,\mathrm{mm}$ renders safe conditions for all three piping systems. The piping steel mass turns out to be smaller than the dead fluid mass, namely 1602, 1467 and 366 kg, cf. Table 3, Khalid [8].

5.5 Selected simulation results

Considering the base isolated single-storey asymmetric building of Fig. 1a, forced by the standard El Centro 1940 seismogram scaled to 0.32 g, convincingly approves the separated action of the low-pass filter and of the three fine-tuned TLCGDs, Fig. 6.

The delayed response of any passive absorber system to early peaks in the forcing function is also recognized in Fig. 6a. Reducing such peaks requires additional active control of the tuned absorbers, for example, rendering the hybrid ATLCGD. Simulations by Hochrainer, see [13] and for the control tools [25], show excellent results by injecting actively controlled gas shots into the gas vessels. However, for practical applications, the problem of removing the injected amount of gas under transient pressure conditions is yet unsolved for the permanently sealed TLCGD. Since the horizontal displacements are localized at the isolation level, we present Fig. 6b for control purpose. Due to the guiding motion provided by the novel isolation element the small induced vertical motion is directly proportional to the horizontal one, the factor is the tangent of the small tilting angle. Hence, all lifelines connections to the ground must be redesigned with flexible elements, a drawback of that kind of classical base isolation.

The weighed sum $\sum_{i=1}^{6} S_i\,|z_{Si}\,(\omega)|$ of the amplitude response functions of the lightly damped base-isolated building states and the optimized system with three TLCGDs is illustrated in Fig. 7, in the relevant frequency window. The tremendously reduced resonant peaks confirm the effective damping supplied by the liquid absorbers.

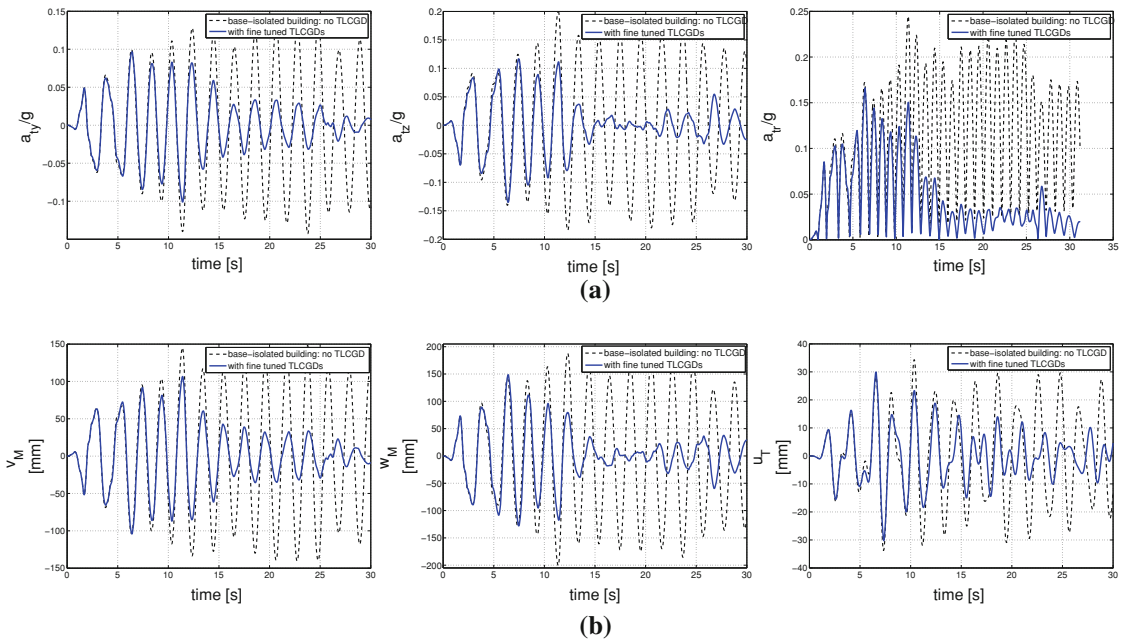

Fig. 6 **a** Total horizontal acceleration of C_M and the resultant a_{tr}. **b** Horizontal displacements and rotation (the vertical one is proportional; factor is the small tilting angle as indicated). Excitation by El Centro, $\alpha_{cr} = 125°$, [8]

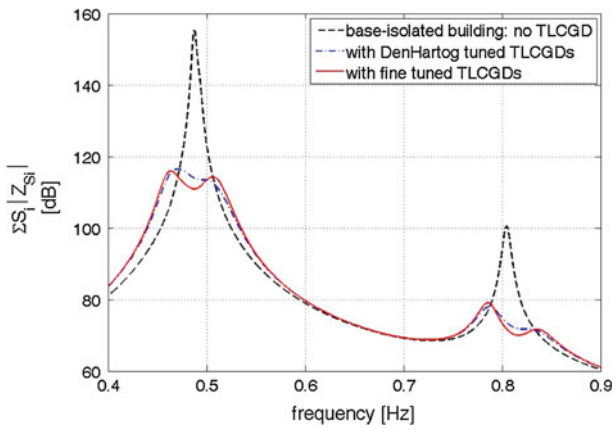

Fig. 7 Weighed sum of amplitude response function (expressed in generalized modal coordinates) for the base-isolated building with and without three TLCGDs installed, $\alpha_{cr} = 125°$, [8]

6 Conclusions

Simulations approve the novel base isolation system consisting of base isolation elements of low horizontal stiffness, with effective damping of the remaining base isolation modes supplied by economical and durable TLCGDs. By transforming the readily available optimal parameters of the TMD of the spring-mass-dashpot type, tuning of these liquid absorbers is done at once in the design stage. Subsequently, fine-tuning in state space renders the optimal absorber frequencies slightly changed; however, the equivalent linear damping turns out dramatically lowered, possibly even saving use of any orifice plates in the piping system. The increased fluid strokes are welcome since there are no moving mechanical parts. In case of too large cross-sectional areas of the piping system, smaller fine-tuned units in parallel action provide an even more robust damping in an extended frequency window around the structural resonance frequency. As experimentally verified, the averaged turbulent damping of the (relative) fluid flow even improves the reduction of the simulation results originally derived with the equivalently linearized damping. Further, this nonlinear damping together with the weakly nonlinear gas compression render the safe design of TLCGD against overloads, mainly due to

the detuning process. Separately arranged sliding elements without continuous energy dissipation supply the necessary amount of static friction to resist the motion of isolation system in case of sufficiently small disturbances. Likewise to the classical base isolation by low-pass filters, buildings with a fixed-base fundamental frequency above 1 Hz are perfectly suited. Contrary, high-rise buildings and their isolation might require a completely different philosophy: Such an important attempt should be mentioned, namely the consideration of "nonlinear internal resonance" by adding a small mass to the foundation interconnected by a nonlinear spring, Vakakis et al [26]. However, in this reference [26] only in-plane story drifts have been considered including a rocking motion. Its generalization to asymmetric buildings is not easily visible.

Acknowledgments Financial support during the four-year period of PhD studies at TU-Vienna by the Higher Education Commission (HEC) of Pakistan via Österreichischer Austauschdienst (ÖAD) in Vienna, is gratefully acknowledged by the first author. Special thanks go to Dr. Rudolf Heuer, Head of the well-equipped Laboratory of the Institute of Building Construction and Technology of TU-Vienna for the provision of laboratory equipments and his valuable guidance in the course of experimental investigations.

References

1. Naeim, F., Kelly, J.M.: Design of Seismic Isolated Structures. Wiley, New York (1999)
2. Buckle, I.G., Mayes, R.L.: Seismic isolation history: application and performance—a world review. Earthq. Spectra **6**, 161–201 (1990)
3. Kunde, M.C., Jangid, R.S.: Seismic behavior of isolated bridges: a-state-of-the-art review. Electron. J. Struct. Eng. **3**, 140–170 (2003)
4. Dowrick, D.J., Cousions, W.J, Robinson, W.H., Barbor, J.: Recent developments in seismic isolation in New Zealand. In: Proceedings of 10th World Conference on Earthquake Engineering (10 WCEE), vol. 4, pp. 2305–2310. Balkema, Rotterdam, ISBN 9054100648 (1992)
5. Giuliani, G.C.: Design experience on seismically isolated buildings. Nucl. Eng. Des. **127/3**, 349–366 (1991)
6. Jolivet, J., Richli, M.H.: Aseismic foundation system for nuclear power stations. In: Proceedings of SMiRT-4, Paper K.9/2, San Francisco, CA (1977)
7. Bachmann, H.: Seismic upgrading of a fire-brigade building by base isolation in Basel, Switzerland. Struct. Eng. Int. **20**(7), 268–274 (2010)
8. Khalid, B.: Control of seismically forced vibrations of asymmetric buildings by means of a novel base isolation system. Vienna University of Technology, Dissertation, Full text available. http://www.ub.tuwien.ac.at/diss/AC07809200.pdf (2010)
9. Khalid, B., Ziegler, F.: Experimental verification of control of asymmetric building vibrations by tuned liquid column gas dampers. In: Proceedings of the 3rd International Conference Experiments/Process/SystemModeling/Simulation, Optimisation. Athens, CD-ROM paper: epsmso09_142.pdf. http://epsmso.gr/2009/default.htm (2009)
10. Khalid, B., Ziegler, F.: A novel base isolation system for asymmetric buildings effectively damped by tuned liquid column-gas dampers. In: Proceedings of the 14th European Conference on Earthquake Engineering (14 ECEE), p. 8, Ohrid, Macedonia, CD-ROM paper (2010)
11. Ziegler, F., Khalid, B.: A novel base isolation system for asymmetric buildings in seismic active zones: damping supplied by tuned liquid column-gas dampers. In: Belyaev, A. K., Irschik, H., Krommer, M. (eds.) Advanced Dynamics and Model Based Control of Structures and Machines, Springer, Vienna (2011, in press)
12. Den Hartog, J.P.: Mechanical vibrations, Reprint, 4th edn. McGraw-Hill, New York (1956)
13. Hochrainer, M.J., Ziegler, F.: Control of tall building vibrations by sealed tuned liquid column dampers. Struct. Control Health Monit. **13**, 980–1002 (2006)
14. Chopra, A.K.: Dynamics of Structures. Prentice-Hall, New Jersey (1985)
15. Clough, R.W., Penzien, J.: Dynamics of Structures, 2nd edn. McGraw-Hill, New York (1993)
16. MATLAB User Guide: Control Toolbox, version 7.8.0. MathWorks Inc., Natick (2009)
17. Fu, C., Ziegler, F.: Vibration prone multi-purpose buildings and towers effectively damped by tuned liquid column gas dampers. Asian J. Civ. Eng. **10**, 1, 21–56 (2010)
18. Ziegler, F.: Mechanics of Solids and fluids, Corr. 2nd edn. Springer, New York (1998)
19. Parkus, H.: Mechanik der Festen Körper, 2nd edn. Springer, Vienna (1996)
20. Reiterer, M., Ziegler, F.: Bi-axial seismic activation of civil engineering structures equipped with tuned liquid column dampers. J. Seismol. Earthq. Eng. (JSEE) **6**(3), 45–60 (2004)
21. Ziegler, F.: Special design of tuned liquid column-gas dampers for the control of spatial structural vibrations. Acta Mech. **201**, 249–267 (2008)
22. Warburton, G.B.: Optimum absorber parameters for various combinations of response and excitation parameters. Earthq. Eng. Struct. Dyn. **10**, 381–401 (1982)
23. Müller, P.C., Schiehlen, W.O.: Lineare Schwingungen. Akademische Verlagsges, Wiesbaden (1976)
24. Young, W.C: Roark's Formulas for Stress & Strain, 6th edn. McGraw-Hill, Prentice Hall, Singapore (1989)
25. Soong, T.T.: Active Structural Control: Theory and Practice. Wiley, New York (1990)
26. Vakakis, A.F., Kounadis, A.N., Raftoyiannis, I.G.: Use of non-linear localization for isolating structures from earthquake-induced motions. Earthq. Eng. Struct. Dyn. **28**, 21–36 (1999)